

Design Additional Shielding for a PHDS Germanium Gamma-ray Imager (GeGI)

Madison Allen¹, Sam Farmer¹, Terra Holly¹, Melody Monzo¹, Adam Caswell²

¹University of Tennessee Knoxville, Knoxville, TN 37996, (mmonzo@vols.utk.edu)

²UCOR, 701 Scarboro Road, Oak Ridge, TN 37830, (adam.caswell@orcc.doe.gov)

INTRODUCTION

A. Background

United Cleanup Oak Ridge LLC (UCOR) is a leading Department of Energy (DOE) contractor located in Oak Ridge, TN. UCOR focuses on the safe and efficient cleanup of unused, contaminated facilities to help restore the Oak Ridge Reservation. When dealing with contaminated facilities, workers are not always aware of what they are walking into when it comes to the nuclear material contained within these structures. To ensure safety, UCOR must be well equipped with technology that can identify nuclear material present with accuracy and precision.

The Germanium Gamma-ray Imager (GeGI) is a portable instrument used to detect and locate nuclear materials using rapid scanning and high-resolution spectroscopy. Figure 1 shows an image of the GeGI detector.



Fig. 1. GeGI detector at UCOR. [1]

The GeGI provides two types of imaging capabilities: Compton imaging and pinhole imaging. Figure 2 shows the difference between images produced by Compton and pinhole imaging. While both types are useful for different measurement situations, the main focus of this project is to improve the performance of pinhole imaging by designing supplemental shielding. Compared to Compton imaging, pinhole imaging has a higher spatial resolution, which provides more precise information regarding the source, source location, and spatial distribution.

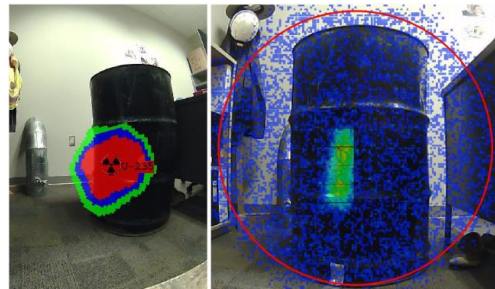


Fig. 2. (Left) Image produced from Compton mode. (Right) Image produced from pinhole mode. [2]

Currently, when using pinhole imaging capabilities, the GeGI is unable to pinpoint the location of nuclear materials when used in high background environments. This issue is due to the detector only providing proper shielding for the front side of the detector, but not for the sides or back of the detector. With the current shielding, the sensitivity for detecting gamma radiation in front of the detector is low, while the sensitivity for the back of the detector is high. With proper shielding to the back of the detector, the detector's sensitivity for the background can be decreased, while the radioisotopes in the foreground can be effectively located and measured.

Understanding these limitations, the purpose of this project is to provide additional modular shielding for the Germanium Gamma-ray Imager (GeGI) to ensure accurate readings and to minimize the shielding material needed.

B. Design Constraints

The design team has developed a structure and strategy to fully shield UCOR's PHDS Germanium Gamma-ray Imager (GeGI) during the use of its pinhole imaging mode while minimizing the weight of the structure.

To meet this goal, certain design constraints were to be kept in mind during the project. These include

- Modular design
- Shielding Material: Lead
- Weight Limit: 35 pounds per piece
- Shielding a maximum energy of 662 keV

- Budget: \$5,000

Modular shielding is based on the idea that the design needs to be used in various environments that require different amounts of shielding while not exceeding the weight limit constraint. The modular ability to have multiple pieces satisfies the above-mentioned weight limit. Keeping the shielding in different thicknesses also allows it to effectively shield a wider range of energies for increased versatility. The energies of focus for this idea can be seen in orange in Figure 3 below. This makes it so that the shielding can cover low and high energies.

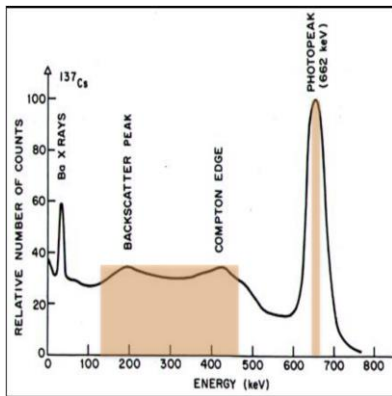


Fig. 3. Compton Continuum with shaded energies of interest for this project.

One of the energies of concern is the photopeak of a Cesium-137 source, seen on the right side of the plot in Figure 3. The shielding structure needs to be optimized to shield incident gamma radiation up to an energy of 662 keV using the pinhole imaging mode. This then sets the maximum energy that the additional shielding needs to withstand. The reason for shielding up to 662 keV is that the front-mounted collimator has the ability to provide adequate shielding up to 662 keV. This is stated in the detector specifications from the manufacturer. Lead, the most effective material to meet these two constraints, was the selected shield material. From the previous team, GGS, lead was chosen as the shielding material since it yielded the lowest estimated total mass. The downside to lead is that it is a heavy material. This brings concern to another constraint of keeping each piece of the shielding material under 35 pounds. This parameter comes from UCOR worker safety. Each worker is allowed to lift a maximum of 35 pounds before they would have to have another worker help them lift the object.

In a high background environment, it is important to keep the exposure as low as possible. Keeping the shielding under the weight limit allows one worker to be able to mount the entire system alone. This makes the workers have an easier time getting the

imager to the areas that it needs to be in. The detector will be portable and easy to move. The final constraint is to keep the design under \$5,000. The design needs to be able to fit each of these constraints moving forward in the project process.

Pinhole imaging utilizes a front-mounted collimator consisting of an inch of lead with a field of view of 60 degrees. In general, the pinhole imaging mode filters detector events so that only single-event, full-energy photon deposition interactions contribute to the resulting image. Figure 4 displays a visual representation and explanation of the sensitivity issue associated with pinhole imaging.

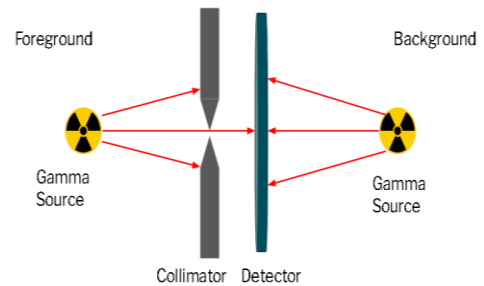


Fig. 4. Foreground versus background sensitivity using pinhole imaging mode.

The overall goal and desired outcome are to design supplemental shielding for the GeGI detector to improve the pinhole imaging resolution in high background radiation environments under the constraint of a weight limit. An optimal geometry and optimal thickness layout for the shield structure are being determined to minimize the amount of unwanted background radiation being detected by the pinhole imaging mode. In doing so, the intention is to optimize the shielding structure to achieve the most effective shield performance of the GeGI detector while minimizing the shielding weight.

The performance requirements of the project include the measurement of the increase in shielding effectiveness that the structure provides, verification that the structure's weight falls within the weight constraint, and the development of a test bed that can represent the shield design to validate the calculations using an experimental approach. In addition, a final 3D-printed model of the newly designed shielding structure for the GeGI detector will be created. The purpose of the 3D-printed model is to verify the physical fitment of the parts and pieces and to serve as a visual representation of the structure. Overall, in developing a shielding structure for this detector, the imaging quality and accuracy from the pinhole imaging mode will be improved while the usability and portability of the detector will not be significantly degraded.

C. Regulations, Standards, and Ethics

For this project, it is essential to follow the existing regulations found in the following documents: Occupational Radiation Protection (10-CFR-835) [3], the National Institute for Occupational Safety and Health (NIOSH) Lead Exposure Limits [4], and the American Conference of Government Industrial Hygienists (ACGIH) Lifting Threshold Limit Values (TLV) [5]. 10-CFR-835 outlines the occupational radiation protection requirements, where this project focused on the radiation exposure limits, worker expectations, controls, and response to potential radiation hazards during the detector's use. The limit specified in 10-CFR-835 is an annual committed effective dose of 5 rem, which was not exceeded during this project in the experimentation phase. It was an important task to limit the dose to as low as reasonably achievable (ALARA) by protocols outlined in 10-CFR-835. For this project, the main material used for the shielding design is lead. The lead exposure limits are outlined in the NIOSH Lead Exposure Limits, which dictate the amount of time spent with the exposed lead material and any potential airborne particles from the material. According to the NIOSH Lead Exposure Limit, the recommended limit is an average of 50 micrograms per cubic meter of air over 8 hours. Since the lead would be coated properly with paint or another material when the design would be manufactured, there is no risk of lead exposure through inhalation or any other method of exposure. The main limitation of this project is based on the worker lifting limits. The ACGIH Lifting TLV defines the maximum weight a worker is allowed to lift, which will apply to lifting and installing each part of the equipment set up, including the shielding material. These limits require each piece of the lead shielding to be no more than 35 pounds to comply with these regulations.

D. Resources

The resources utilized for the shielding design project include MCNP radiation transport software, Solidworks 3D CAD design software, Excel, Python software for thickness optimizations and plotting, the GeGI detector itself for field testing, the vendors, as well as access to 3D printing capabilities. The previous senior design team, GGS, provided information on the selection of lead as the shielding material. Furthermore, the experimental work of creating a test bed required resources such as access to the UCOR facility for testing, steel sheets owned by UCOR for the test bed shielding material (which was converted to the lead equivalency calculated), the detector and cesium-137 gamma sources for experimentation. In addition, the resources for this project also include the design team mentor, Adam

Caswell of UCOR, additional UCOR employees, and graduate students at UTK.

DESIGN

A. Initial Design Ideas

Over the course of the semester, multiple design approaches were considered. Keeping the design constraints in mind, the first design idea included using a progressive shield that would gain thickness as it grew closer to where the background source would interact. This involved having a base layer of lead around the detector, where additional sheets could be concentrated where the background source is strongest. This would involve fabricating thin sheets of lead, placing them in a bracket around the detector, and securing the sheets so they do not move. This would require a structure to be made around the detector that could support the weight of the lead and the fastening system. Figure 5 shows the rough sketch for the structure design.



Fig. 5. Structure design idea with detachable shielding layers. [2]

The lead required for this design would come in various thicknesses, adding another layer of potential error to the process of securing and protecting the detector. This design would be modular, while the simple plates would keep it cost-effective. Additionally, the plates could be adjusted to block higher or lower energy gammas based on the configuration of the plates used. Although this option was considered to be versatile, budget-friendly, and remain under the 35 lb weight limit, this design was not selected based on potential structural issues with the use of multiple layers of lead. Since safety is a priority to the sponsor, a different idea was proposed that could rely on the structural integrity of hardware that had gone through extensive manufacturer testing.

B. Final Design

Throughout the design process, one consistent concept was that each design idea would involve having a versatile shielding setup that could be adjusted to the

amount of shielding thickness needed. With the budget constraint in mind, the design needed to be relatively simple to manufacture to reduce production costs. With these things in consideration, the final design idea entailed having multiple “house” shaped pieces lined up side by side to shield the top and sides of the detector, while a custom-fit back piece would shield the backside of the detector. It was determined the house-shaped design would reduce the amount of lead needed while remaining within budget.

In addition, it was determined that the design would be divided into two layers. The layered shielding design would be versatile enough to be used in low or high-background environments as requested by the sponsor. Additionally, the layers ensure each piece of shielding is under the 35 lb weight limit, which requires only one worker to be present to move each piece.

C. Shield Layer Thickness Determination

To minimize the shielding weight, the design is based on the idea of having two shielding layers: the base scatter layer and the direct view layer. The base scatter layer is the minimum shielding thickness required to block low-energy gammas between 130 keV and 475 keV on the Compton Continuum. The direct view layer is the additional layer that sits on top of the base scatter layer to shield gammas with energies of 662 keV from the full energy peak of Cs-137.

The thickness of each layer will be determined by writing a Python code that uses the attenuation coefficients of lead at different energies to determine the amount of lead needed to stop most of the incoming gamma rays. Using Equation 1, seen below, a thickness could be calculated based on the attenuation coefficients of lead at different energies.

$$I = I_0 e^{-\mu x} \quad (1)$$

Where:

I = Intensity of gamma radiation with shielding

I_0 = Initial intensity of the gamma radiation

μ = Attenuation coefficient

x = Thickness of the lead shield

To use this equation, multiple values are needed. The first values needed are the attenuation coefficients of lead at different energies. These attenuation coefficients are important to the calculation as these values determine how much energy the particles

lose as it travels through the shielding material. They act as the backbone of the equation, allowing a thickness to be found. These coefficients were found with the NIST XCOM [6] tables for attenuation values of each element. Lead was then selected and all of the available values were used up to the maximum shielding energy of 662 keV. This list was incomplete so there was a need to interpolate some of the values. This was done by using a function in Python [7] to do a linear interpolation for energies that fell within gaps of the tabulated values. With all of the attenuation values able to be found, an energy range was selected. As stated, the large range of concern was 130 keV to 474.6 keV. This was then set as the upper and lower range on a Gaussian distribution with roughly 250 keV being the median value. A loop was then created to pull random energy values from the 130 to 474.6 keV range while the code is running. These energy values were then matched with their respective attenuation values. With the attenuation values and energies matched, another equation is needed. Equation 2 shows the attenuation ratio equation used to find the optimal thickness of the lead.

$$A_{theor.} = 1 - e^{-\mu x} \quad (2)$$

Where:

$A_{theor.}$ = Attenuation ratio

Here, $A_{theor.}$ is the ratio of the incoming radiation intensities. Specifically, the attenuation ratio is a measure of how easily a certain material can be penetrated by incident radiation. This ratio was set to 0.85, or 85%, as a starting point. This blocks most of the incoming radiation, only allowing 15% of the radiation to pass through into the detector. This low amount of radiation would not decrease the image quality of the pinhole imaging mode. Once this ratio was decided upon, the code was run multiple times to find an average thickness value. On top of this base thickness, there was a need for a thicker layer to go over the first layer to block the full 662 keV peaks. This was decided by changing the attenuation ratio to 90%. Once the code was run for this value, the thicknesses in Table 1 were obtained.

TABLE 1: Thickness of Lead Shield Layers

Layer	Thickness (in)	Attenuation Ratio
Base Scatter (130 - 474.6 keV)	0.1979	85%
Direct View (662 keV)	0.7000	90%
Total	0.8979	95%

Here it can be seen that 0.1979 inches of lead will attenuate 85% of the incoming radiation. This will cover the 130 to 474.6 keV energy range. The 0.7000 inches of lead will attenuate 90% of that radiation. This covers the higher energy of 662 keV. With both layers combined, the radiation is cut by 95%. This greatly improves the image quality in the pinhole imaging mode.

D. Final Design & Modeling

Using the Python code referenced above, the base scatter layer thickness was determined to be 0.1979 inches, while the direct view layer was determined to be 0.7000 inches. Using the determined thickness, the base scatter layer, which will act as the base shielding layer, was modeled in Solidworks and is shown in Figure 6 below.

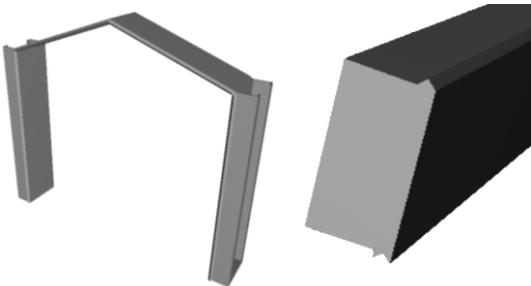


Fig. 6. House shape shielding base (left) and a close-up of interlocking edges (right).

Once again, the house-shaped design is meant to maximize the shielding effectiveness, while also minimizing the amount of lead needed. By creating the peak, the amount and weight of the shielding can be reduced. Looking at the model, the peak of the house is at a more relaxed angle. After going over the design with the vendors, they explained that a more dramatic angle would be difficult to reproduce in a manufacturing environment. Taking this into consideration, the design was adjusted to the manufacturing constraints. The change in angle was not considered to have negative effects on the function of the design or design criteria.

Since the house-shaped design is made up of two layers of plates, a channel was added to the base scatter layer. As shown in Figure 6, the part has edges on the sides, which will act as both a channel and support for the additional layer of shielding to slide into place. This channel, or bracket, will ensure the added layer remains securely in place to maintain worker safety. The channel will be made out of steel and attached to the lead shielding during the manufacturing process. After speaking with the vendor, the channels will most likely be attached with a strong industrial-grade adhesive. Since the detector will not be turned at extreme angles sideways or upside down, it was determined that an additional fastening for the top of the house-shaped design was not required. With this in mind, the design can rely on gravity to secure the pieces in place. Furthermore, there will not be brackets added to the top to secure the added layer.

To ensure there is no gap between the shielding parts, an interlocking edge was added to the side of each base part. A diagram of how the interlocking edges will look and fit is shown in Figure 7.



Fig. 7. Interlocking shielding edge diagram.

This edge was added to all the base layers so that when put next to each other they would interlock. The interlock will ensure that there is no leakage between the shielding pieces.

For the additional house layer or direct view, the piece will look identical to the one shown in Figure 6 except it will not contain channels on the sides. The direct view layer for the house-shaped design can be seen in Figure 8.

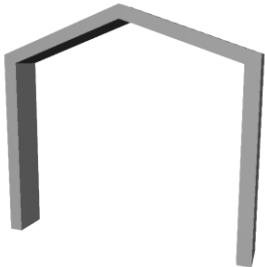


Fig. 8. House shape shielding direct view layer.

When this additional piece is added, the two layers combine to a total thickness of 0.898 inches, which can shield the 662 keV photopeaks of Cs-137.

When added, this layer allows the shielding thickness to be adjusted for use in high background environments. This piece is dimensioned to fit over the house shape base layer, where it will slide and sit in the steel channel. The next piece designed was the back piece. Figure 9 shows the back base scatter and direct view layers, which both contain a cut-out for the power cord.

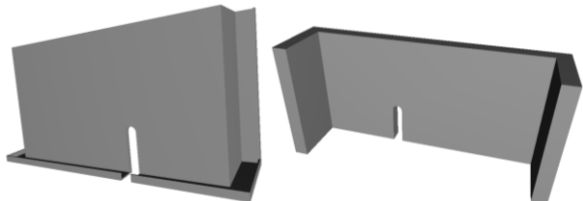


Fig. 9. Back base scatter shielding (left) and direct view layer (right).

Since the cut-out is such a small portion of the backside, there are no concerns that the shielding effectiveness will be compromised. The back part is also shorter in height to maintain under the weight restriction. The back base layer is designed the same as the house base, where there will be steel channels added on the sides. This channel will also support and secure the additional layer of shielding, which is also shown in Figure 9. The direct view layer will slide into the channels, just like the house-shaped part, and is also equipped with interlocking edges. Overall, the part dimensions were determined with consideration for the size of the detector, added space for the hardware, and weight restrictions.

In order to attach the shielding pieces to the base plate of the detector, holes for mounting the hardware will need to be added to the shielding design in the future. The hardware chosen allows for different amounts of shielding material to be added to the detector. The chosen hardware can be seen in Figure 10 below.

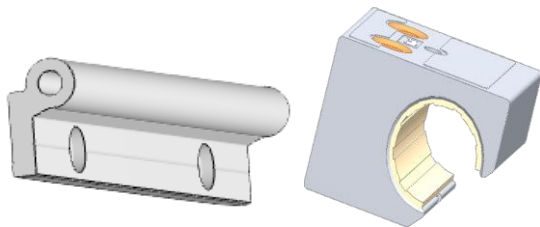


Fig. 10. Rail System Hardware for the mounting of the shielding. The image (left) is the linear guide system rail. The second image (right) is the pillow block. [8, 9]

As shown on the left, the linear guide system rail is mounted on both sides of the detector’s base plate and weighs 1.37 lbs/m. The railing length runs along the

side of the base plate and extends in the back, where the total length will be about 0.381 m. The total weight of one rail is about 0.52 lbs, which will not affect the weight of each part. To connect the shielding pieces to the railing, the pillow block shown in Figure 10 is attached to both of the insides of each piece, where the weight is 0.11 lbs. This allows pieces to glide on and off of the rail, making the amount of shielding pieces completely adjustable. In total, there will be two pillow blocks added to each base part, which will add a total of 0.21 lbs to each piece. In addition, each piece is set right up against the edge of the pieces next to it with an interlocking edge as mentioned.

Using an Excel sheet, the weight for each part including the attached hardware was calculated. The weights of each part are shown in Table 2.

TABLE 2: Total Calculated Weights of Shielding Parts

House Base Scatter (lbs)	House Direct View (lbs)	Back Base Scatter (lbs)	Back Direct View (lbs)	Total Weight (lbs)
4.87	22.64	3.30	31.69	145.00

Looking at the values in Table 2, the weight for each part including the hardware is under the weight requirements of 35 lbs. This allows there to be a margin of error for any differences in the actual weight of the manufactured parts. The total weight of all the shielding and hardware was determined to be 147.10 lbs, where a cart will be used with a weight limit of over 300 lbs. By mounting the hardware to the baseplate, the total weight of the shielding will be applied to the detector mount and cart. This ensures that the worker lifting limits will not be exceeded and safety concerns are minimized.

3D-PRINTING

To show a model of the final design, the decision was made to 3D print the detector, baseplate, hardware, and shielding. This was done with the resources available at the Innovation and Collaboration Studio (ICS) in the Zeanah Engineering Complex. To do this, 3D models of the modular design were made in Solidworks and Autodesk Inventor which were then scaled down to 66% of the original size to meet the constraints of the 3D printers. Each part of the design was printed at the same scale to ensure the pieces can fit together as intended. To print these parts, the 3D models used were from the manufacturer of the GeGI detector, the hardware manufacturer, and the shielding design models made by the team. Figure 11 shows the final 3D-printed models, which include the printed models and

the scaled versions of the detector and baseplate. The shielding setup includes a total of four house structures, four house direct view layers, one back base layer, and one back direct view layer. In all, the hardware needed includes two rails and ten pillow blocks.

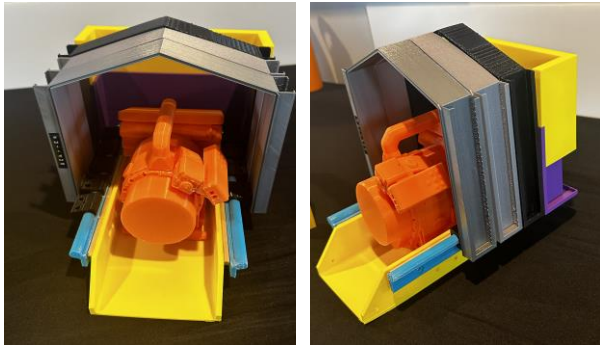


Fig. 11. 3D-Printed Models.

EXPERIMENTAL DESIGN and EXECUTION

For the experimental phase, the objective was to validate calculated attenuation ratios with experimental data. To execute this objective, experimental data needed to be collected to validate calculations and design. Materials necessary for the collection of experimental data are the GeGI detector, a cart, 3 Cs-137 sources, tape, c-clamps, measuring tape, a cardboard box, and steel plates. Since lead was not available for the experiment, steel plates were used, and an equivalency conversion to lead was conducted. A schematic was created to lay out the location of the three sources. Figure 12 below shows the schematic of the layout of the sources.



Fig. 12. Schematic of detector, sources, and shielding arrangement. [2]

One source is in the pinhole imaging field of view (Source A) of the detector, and the other two sources (Sources B and C) were perpendicular to the detector. Source A was taped to the wall in the field of

the detector while the detector was 1 foot away from the wall. Each source was 1 foot away from the detector. The sources were placed on top of the cardboard box. The distance between Source B and C was 4 inches. Source A had an activity of 8.90 microcuries. Source B had an activity of 9.33 microcuries. Source C had an activity of 4.70 microcuries. Once the setup was complete, a finalized procedure was determined to include three different configurations: base, scatter, and total shield. For each configuration, three measurements were taken over a period of 40 minutes. The same source configurations were used for all measurements.

The first measurement was the base configuration. The figure below shows the setup for the base configuration. In Figure 13, a cardboard box is shown on top of the detector. This is due to the assumption of placing steel plates along the cardboard box. However, the cardboard box did not function as assumed. Therefore, the cardboard box was no longer used for the rest of the configurations.



Fig. 13. Set up for Base Configuration.

The second set of measurements was the scatter + direct view layer shield configuration. Figure 14 below shows the setup for the scatter + direct view layer shield configuration. The layout and description of the sources are shown up above in Figure 12. The sources were placed on top of the cardboard box. Since lead was not available for the experiment, steel plates were used. An equivalency conversion from steel to lead was conducted. A total of 6 steel plates were used. Each steel plate was 0.25 inches thick. This created a shielding thickness of 1.5 inches. The steel plates were placed two inches away from the base plate of the detector. This was presumably based on the physical design of the shielding. This setup was used to test the total shield configuration.



Fig. 14. Setup for total shield configuration.

The third set of measurements was the scatter configuration. Figure 15 below shows the setup for the scatter configuration. The layout and description of the sources are shown up above in Figure 12. The sources were placed on top of the cardboard box. Since lead was not easily available for the experiment, steel plates were used. An equivalency conversion from steel to lead was conducted. A total of 4 steel plates were used. Two steel plates were placed two inches from the base plate of the detector. To create a scatter, two steel plates were placed in front of the sources. This setup was used to test the scatter configuration.



Fig. 15. Setup for scatter configuration.

For each configuration, an average of the three repetitions was calculated and plotted for each average spectrum. After each measurement, the statistics were viewed to ensure there weren't any outliers. The experimental attenuation ratio was calculated by dividing the peak area counts for the shielded versus unshielded data sets. This was done for all configurations. For each configuration, a comparison of the experimental and calculated attenuation ratio was done. The next section will go into depth about the results obtained.

RESULTS

The results of the project include shield thickness calculations which were performed to optimize the attenuation ratio of the shield while also reducing the shielding weight. The thickness calculations were performed using specific target attenuation ratios for each thickness layer. After completing the thickness calculations for the entire full shield which is composed of the scatter base layer and the direct view layer, an experiment at UCOR was performed. This experiment was performed at UCOR to validate the thickness calculations as well as the attenuation ratios theoretically determined for each thickness layer of the shield.

Based on the thickness value found previously, there was an attempt to use MCNP to simulate the shielding. Due to time constraints, these efforts were not continued as the focus shifted to Python and finding the results from the experiment. The MCNP model can be seen in Appendix A to understand the progress that was made in this area.

After the thickness calculations were completed, the experiment was executed at UCOR and then experimental data analysis was performed. The scatter layer configuration as well as the unshielded configuration could all be simulated with the corresponding thickness of material from the thickness calculations. For the purpose of experimental testing for the total shield configuration specifically, a lead equivalent of 0.681 inches was used instead of an original one-inch lead equivalent due to the limited number of steel plates present.

After collecting the necessary experimental data from the UCOR facility, experimental data analysis could begin. To perform the experimental data analysis, experimental attenuation ratios were determined by using Python coding. Before averaging together all three datasets for each shielding configuration tested, a statistical check was performed. To perform the statistical check, the standard deviation was calculated for each repetition for each thickness configuration tested by using a standard deviation function in Python. The standard deviation was then determined between the three datasets for each configuration. It was found that all three of the full shield configurations (scatter plus direct view layer) were within one standard deviation from the mean. However, for the scatter base layer configuration, each of the three datasets collected was within three standard deviations from the mean. Lastly, the unshielded bare detector measurements were all found to be within one standard deviation from the mean. Thus, it was determined that there were no outstanding outliers in the three repeated datasets for each configuration.

After the statistical analysis and verification of the validity of the repeated measurements, the three

collected energy spectra measurements were all averaged together. This was performed for all three thickness configurations tested. Next, the plots of radiation count as a function of gamma energy data for the experiment were made in Python. Figures 16, 17, and 18 display the collected results for the unshielded bare detector, the scatter base layer, and the full shield, respectively.

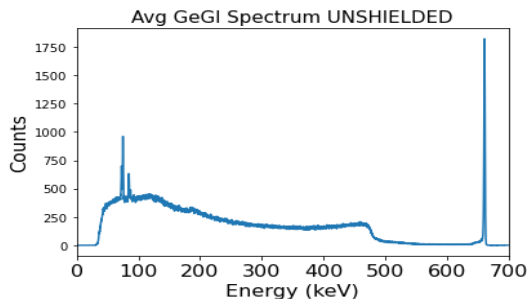


Fig. 16. Unshielded Experimental data collected at UCOR. This plot displays the radiation count data as a function of gamma energy for the unshielded configuration.

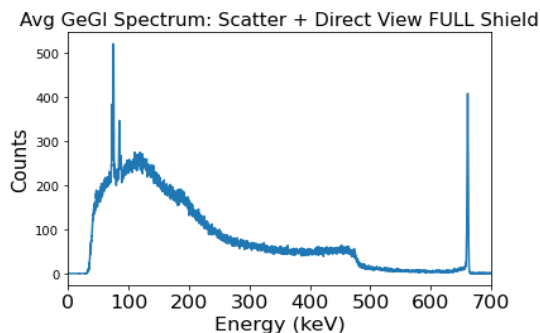


Fig. 17. Full Shield Experimental data collected at UCOR. The plot displays the radiation count data as a function of gamma energy for the full shield configuration.

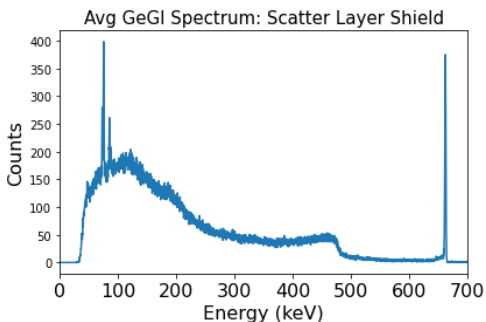


Fig. 18. Scatter Experimental data collected at UCOR. The plot displays the radiation count data as a function of gamma energy for the scatter layer configuration.

The plots displayed in Figures 16, 17, and 18 were all collected by the GeGI detector at the UCOR facility. It can be seen from inspection that all plots follow the same trend which reflects the energy spectrum of cesium-137, the source used for experimental testing.

All plots display the 662 keV photopeaks associated with cesium-137, as well as the low-energy excitation gamma-ray emission, and the Compton Continuum from approximately 130 keV to 475 keV.

Looking at the figures, there are some noticeable differences between the graphs. Specifically, the unshielded configuration had a noticeably higher count than the other two shielded configurations, which is to be expected. When inspecting Figures 17 and 18, it can be seen that the peak at around 75 keV has 100 counts more for the full shield configuration than the scatter. The peak at 75 keV is due to the x-rays from the lead shielding. This is not to be expected and could be due to the inability to truly test for scatter. Regardless of this inconsistency, both shielded configurations had significantly lower counts than the unshielded configuration in Figure 16, which is to be expected. It can also be seen that the count area under the energy spectrum curve specific to the Compton Continuum energy range is smaller for the plots in Figures 17 and 18 than it is for the unshielded configuration in Figure 16. Looking at these graphs, it can be determined that both shielding configurations decreased the number of particles interacting with the detector as intended.

After inspection of the experimental plots, data analysis was then performed in Python to determine the experimental attenuation ratios for the scatter base layer and the full shield (scatter plus direct view layer). To do so, equation 3 below was used to determine the experimental attenuation ratio, A_{exp} . The experimental attenuation ratio was determined for both the scatter layer configuration and the full shield configuration that was tested at the UCOR facility.

$$A_{exp} = 1 - \frac{I}{I_0} = 1 - \frac{Area_{Shielded}}{Area_{Unshielded}} \quad (3)$$

Where:

I = Intensity of gamma radiation with shielding

I_0 = Intensity of gamma radiation without shielding

$Area_{Shielded}$ = Area under the Count Versus Energy Curve for Corresponding Shielded Configuration

$Area_{Unshielded}$ = Count Area under the Count Versus Energy Curve for Unshielded Shield Configuration

* (Compton Continuum energy range - Scatter Configuration
662 keV photopeak Area - Full Shield Configuration)

Before solving for A_{exp} using equation 3, the count area under the spectrum curve was determined. The count area was determined by using a function in Python that utilized Simpson's Rule. This function in

Python uses a set value range to approximate the definite integral (area under the peak curve). The area under the 662 keV photopeak was determined for the full shield experimental attenuation ratio (plot displayed in Figure 17). In contrast, the area under the Compton Continuum energy range from 130 keV to 475 keV was determined for the scatter base layer configuration (plot displayed in Figure 18).

As for the unshielded configuration, the area under the spectrum curve was determined for both the 662 keV photopeak area as well as the Compton Continuum area (plot displayed in Figure 16). After the determination of all the necessary $Area_{shielded}$ and $Area_{unshielded}$ values using Python coding, equation 3 was used to determine the value of A_{exp} , the experimental attenuation ratio. The A_{exp} value for the scatter base layer was determined to be 68.1% and the A_{exp} value for the full shield configuration was determined to be 77.3%.

Before comparing the theoretical to experimental attenuation ratio for the full shield specifically, a calculated value of the attenuation ratio had to be redetermined using the correct corresponding material equivalent used for the experiment. Specifically, to compensate for the discrepancy between the equivalent thicknesses of material for the full shield configuration, an updated calculated value of the attenuation ratio for the total full shield was determined. This value was determined to be 76.4% using the experimental steel-equivalent lead thickness tested in the experiment (1.5 inches of steel or 0.681-inch lead equivalent). Specifically, this value was determined using Equation 2. This contrasts the 95% theoretical attenuation ratio of the full shield (direct view plus scatter layer), determined from a one-inch lead equivalent previously calculated.

TABLE 3: Theoretical and Experimental Results of Shield

Thickness Layer	$x_{calc Pb}$ (in.)	$x_{steel equi}$ (in.)	$x_{steel test}$ (in.)	$A_{theor.}$	A_{exp}	%Difference
Scatter	0.1979	0.435	0.5	85% (for 1" lead equiv)	68.1%	19.9%

Direct View	0.7	1.54	-	90% (for 1" lead equiv)	-	-
Total Shield (Scatter + Direct View)	0.898	1.976	1.5	76.4% (for 1.5" steel equiv)	77.3%	1.13%

In Table 3, the calculated thickness of lead for the scatter baselayer, the direct view layer, and the full shield for the GeGI detector is shown. In addition, the attenuation ratios used to calculate the thickness of each layer are also shown. Afterward, the theoretical to experimental attenuation ratios could then be compared with like material equivalency. In comparing the attenuation ratios of the theoretical and experimental work for the full shield configuration, it was found that there was a 1.13% difference between the A_{exp} and $A_{theor.}$ specifically for the total full shield. These comparisons can be seen in Table 3. This configuration includes both the scatter baselayer and the director view layer. With this significantly low percent difference between the theoretical and experimental values, the validity of the theoretical thickness calculations performed was verified. This confirms that the attenuation ratio equations utilized for designing the shield for the GeGI detector are accurate in determining the appropriate shielding effectiveness.

In comparing the attenuation ratios of the theoretical and experimental work for the scatter base layer configuration, it was found that there was a significantly large percent difference between the two. Specifically, it was determined that there was a 19.9% difference between the A_{exp} and $A_{theor.}$ specifically for the scatter layer configuration. This large percent difference between the theoretical and experimental attenuation ratio for the scatter base layer may be explained by the simplicity of the experimental setup. Properly simulating a radiation scattering event and shielding the radiation can be difficult. To simulate a radiation scattering environment, more material placed in alternate locations of the experimental testing room may be used. This might prove useful to generate more scattering. However, it is generally difficult to experimentally quantify the degree to which scattering occurs when scattering and attenuation of gamma radiation are present simultaneously.

In addition to computationally evaluating the shielding effectiveness through measuring and comparing attenuation ratios, the improved pinhole imaging resolution with the use of additional shielding can be visually seen through the use of the GeGI detector. This can be seen in the below images displayed in Figure 19.

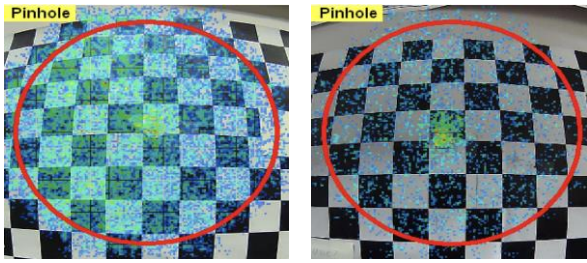


Fig. 19. The left image displays the pinhole image captured by the detector while in the unshielded configuration. The right image displays the pinhole image captured by the detector while in the full shield configuration.

The left image in Figure 19 above is the pinhole image captured by the GeGI detector in the unshielded configuration. The right image in Figure 19 displays the pinhole imaging of the GeGI detector while in the full shield configuration. When inspecting these images, it can be seen that there is considerably more radiation apparent without shielding than with shielding. This is due to the attenuation level of shielding material decreasing the level of radiation counts, specific to the shielded configuration. Furthermore, it can be seen that in both images, a source is in the direct, center view of the detector and two sources are perpendicular to the detector. In addition, it can be seen in the left image of Figure 19 that the exact location of the radioactive source cannot be determined. In the right image, the source radiation is shown more clearly. Based on the images captured and displayed in Figure 19, the pinhole imaging was improved through the use of shielding material. Thus, the addition of the calculated lead-equivalent thickness of the steel used for the experiment did prove to be useful in improving the resolution of the GeGI detector in pinhole imaging mode.

Overall, the results of the theoretical and experimental work of the project did show a significant increase in the shielding effectiveness of the GeGI detector while in pinhole imaging mode. This was confirmed computationally and quantitatively through both theoretical and experimental calculations as well as through the pinhole images captured by the detector.

SUMMARY

The purpose of this project was to design supplemental shielding for the GeGI detector to improve the pinhole imaging resolution in high background radiation environments under constraints. The finalized design concept was to have a versatile shielding setup that could be adjusted to the amount of shielding thickness needed. With this in consideration, the final design idea entailed having multiple “house” shaped pieces lined up side by side to shield the top and sides of

the detector, while a custom-fit back piece would shield the backside of the detector. When the direct view and scatter layer are added together, the total thickness must shield gammas with energies of 662 keV from the photopeak of Cs-137.

The design was created to maximize the shielding effectiveness, which should minimize the number of particles able to interact with the detector. This will allow the pinhole imaging mode to have a better resolution when finding a radioactive source in a highly contaminated environment. To maximize efficiency, lead was chosen as the shielding material used. Since lead is a heavy material, the worker lifting limits was a major design constraint, but the final parts were determined to stay within the desired weight limit of 35 lbs. Considering the budget limitations, the complexity of each part was taken into account to reduce the number of custom parts. Following a recent quote from the vendor, the house-shaped part would cost around \$2,000 to manufacture. The cost of all the hardware needed will be \$500, making the current cost \$2,500 for all the hardware and the house-shaped part. Although this does not include all the parts required, the price of parts will decrease as the amount ordered increases. Each of these factors and restrictions were taken into consideration when creating the final shielding design, while also enhancing the efficiency of the pinhole imaging mode. In all, the design was able to meet all of the requirements outlined by the sponsor and the models created are ready to be sent out to the vendor for an updated quote. With the finalized shielding design, an experimental phase began.

For the experimental phase, the objective was to validate calculated attenuation ratios with experimental data. To execute this objective, an experimental procedure had to be thought out to validate calculations and design. Once the setup was complete, a finalized procedure was determined to include three different configurations: base, scatter, and total shield. The results of the project include shield thickness calculations which were performed to optimize the attenuation ratio of the shield while also reducing the shielding weight.

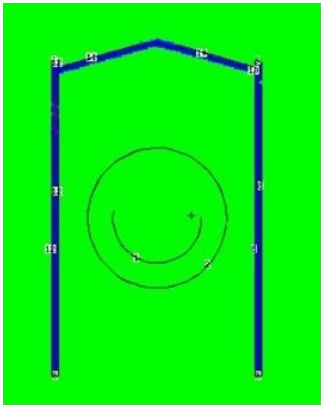
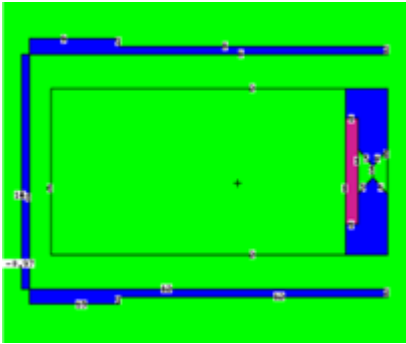
Overall, the results of the theoretical and experimental work of the project showed a significant increase in the shielding effectiveness of the GeGI detector while in pinhole imaging mode. This was confirmed computationally and quantitatively through both theoretical and experimental calculations as well as through the pinhole images captured by the detector. In developing a shielding structure for this detector, the imaging quality and accuracy from the pinhole imaging mode improved while the usability and portability of the detector will not be significantly degraded.

FUTURE WORK

Using the finalized design models, the design will be sent to the vendor for a new quote to be requested. The hardware for the railing system will be ordered. For the experimental section, future work can be done by collecting data for the scatter configuration. A new configuration for the scatter attenuation ratio by testing only with the scatter shield next to Sources B and C and no shield next to the detector. This new setup could provide better scatter measurements.

APPENDIX A

MCNP simulations to model the shielding design are displayed below.



5. "TLV/BEI Guidelines." *ACGIH*. <https://www.acgih.org/science/tlv-bei-guidelines/>.
76. Berger, M. J. "NIST XCOM: photon cross sections database." <http://www.nist.gov/pml/data/xcom/index.cfm> (2010).
7. Jonathan Mitchell. "Python Code Documentation." October 14, 2021.
8. "Drylin® W Single Rail WS." <https://www.igus.com/product/736?artNr=WS-10>.
9. "Iigus® CAD." <https://www.igus-cad.com/default.aspx?cul=en-US&ArtNr=WJ200UM-01-16-AL&mandant=USA¶mmode=>.

REFERENCES

1. "The GeGI | The World's Most Sophisticated Gamma RayDetector." [Online]. Available: <https://phdsco.com/products/gegi>. [Accessed: 07-Mar-2022].
2. A. G. Caswell, NDA GeGI Shielding Project Additional Info 2022-2023 PowerPoint, Oak Ridge
3. "10 CFR Part 835 -- Occupational Radiation Protection." <https://www.ecfr.gov/current/title-10/chapter-III/part-835?toc=1>.
4. "CDC - NIOSH Pocket Guide to Chemical Hazards - Lead." <https://www.cdc.gov/niosh/npg/npgd0368.html>.